ARTICLES

Journal of Semiconductors
(2020) 41, 092701
doi: 10.1088/1674-4926/41/9/092701

Highly-rough surface carbon nanofibers film as an effective interlayer for lithium–sulfur batteries

Hongfan Zhu[1], Mo Sha[1, 2], Huaping Zhao[2], Yuting Nie[1], Xuhui Sun[1, †], and Yong Lei[2, †]

[1]Institute of Functional Nano and Soft Materials (FUNSOM), Jiangsu Key Laboratory for Carbon-Based Functional Materials and Devices, Collaborative Innovation Centre of Suzhou Nano Science and Technology, Soochow University, Suzhou 215123, China

[2]Fachgebiet Angewandte Nanophysik, Institut für Physik & IMN MacroNano® (ZIK), Technische Universität Ilmenau, Ilmenau 98693, Germany

Abstract: Lithium–sulfur (Li–S) battery with a new configuration is demonstrated by inserting a flexible nitrogen-doping carbon nanofiber (N-CNFs) interlayer between the sulfur cathode and the separator. The N-CNFs film with high surface roughness and surface area is fabricated by electrospinning and a subsequent calcination process. The N-CNFs film interlayer not only effectively traps the shuttling migration of polysulfides but also gives the whole battery reliable electronic conductivity, which can effectively enhance the electrochemical performance of Li–S batteries. Finally, Li–S batteries with long cycling stability of 785 mAh/g after 200 cycles and good rate capability of 573 mAh/g at 5 C are achieved.

Key words: Interlayer; N-CNFs; Li–S battery; electrospinning

Citation: H F Zhu, M Sha, H P Zhao, Y T Nie, X H Sun, and Y Lei, Highly-rough surface carbon nanofibers film as an effective interlayer for lithium–sulfur batteries[J]. *J. Semicond.*, 2020, 41(9), 092701. http://doi.org/10.1088/1674-4926/41/9/092701

1. Introduction

Due to the rapid development of electrical vehicles and portable electronic devices, rechargeable batteries with low-cost and high energy density are in great demand[1–6]. Unfortunately, the currently commercial lithium-ion batteries suffer from limited energy density. Therefore, developing next-generation of rechargeable batteries with higher energy density is necessary. Lithium–sulfur (Li–S) batteries are one of the most promising technologies to meet higher energy demands due to the cost-effective and environmentally sulfur cathode that provides a high theoretical capacity of 1675 mAh/g and a high theoretical energy density of 2567 Wh/kg[7, 8]. However, to enable Li–S batteries becoming a commercial technology, there are still many challenging issues required to be addressed, for example, fast capacity degradation, poor rate stability, and low Coulombic efficiency of current Li–S batteries, resulting from the high solubility of polysulfide intermediates (Li_2S_n, $4 \leqslant n \leqslant 8$) in organic electrolytes, the insulating nature of sulfur, and the huge volume expansion during cycling, respectively[9–11].

So far many strategies have been proposed to address these abovementioned obstacles with the majority focusing on the cathode modification, such as embedding sulfur in/on various forms of carbon or surface coating of sulfur with conductive polymers or oxides[12–15]. Although the cathode modification could optimize the electrochemical performance of Li–S batteries, the complex and expensive process of cathode modification limits the feasibility of commercializing Li–S batteries in the future[16–18]. Therefore, more effective approaches are still necessary to be developed. One of the promising alternative strategies is to insert a functional interlayer between the cathode and the separator to intercept the diffusing polysulfides during charging-discharging process[19–22]. The introduction of a functional interlayer is expected to effectively enhance the utilization of active materials by trapping and stabilizing the high solubility of polysulfides at the cathode and finally improve the performance of Li–S batteries. Till now, there have been several preliminary investigations about the design and fabrication of the functional interlayer, such as carbon, polymer and metal oxide-based interlayers[23–25]. Among them, carbon-based interlayers, such as porous carbon[26, 27], carbon nanotube[28, 29], graphene[30, 31], carbon nanofibers (CNFs)[24, 32], have particularly attracted much attention due to their low-cost, high conductive and physical adsorption for the dissolved polysulfides. For example, Singhal *et al.* fabricated different porous CNFs films as interlayers and studied the effect of surface area on the electrochemical performance of Li–S batteries[24]. The results revealed that high surface area can deliver a high discharge capacity and capacity retention. However, due to the smooth surface of CNFs, the ability of adsorption and tapping for polysulfide is limited, leading to parts of polysulfides being dissolved in the electrolyte and thus decreasing the electrochemical performance of Li–S batteries. Therefore, improving surface roughness of CNFs should be an effective method to increase the surface area, and the rough surface can trap and stabilize the sulfur on the cathode and reduce the dissolution of polysulfides. Unfortunately, few researches have been focused on increasing the surface roughness of CNFs. Therefore, porous CNFs membranes consisting of CNFs with highly-rough surface as interlayers for Li–S batteries will benefit to decreasing the dissolution of polysulfides and increasing electrochemical performance.

Electrospinning is a simple fiber formation technique that applies a strong electric field to pull or thin out a poly-

Correspondence to: X H Sun, xhsun@suda.edu.cn; Y Lei, yong.lei@tu-ilmenau.de

Received 20 JULY 2020; Revised 4 AUGUST 2020.

mer solution or melt jet forming nanofibers and these nanofibers inherently constitute a free-standing non-woven nanofiber mat[33–35]. In this work, we use the ordered mesoporous carbon (CMK-3) to package sulfur powder as the cathode and employ electrospinning to synthesis novel N-doped CNFs with highly-rough surface as the functional interlayer. Polyacrylonitrile (PAN) and polyvinylpyrrolidone (PVP) are solutes to prepare electrospinning precursors for electrospinning. According to the different pyrolysis temperatures of PAN and PVP, we annealed the as-spun PAN/PVP nanofibers at a specific temperature to decompose PVP which degrades at a much lower temperature than that of PAN, getting the nitrogen-doped CNFs (N-CNFs) film. With N-CNFs films as functional interlayers in Li–S batteries, CNFs with highly-rough surface can intercept and stabilize soluble polysulfides and the N-doping can improve the electronic conductivity of the CNFs, which leads to the improvement in electrochemical performance of Li–S batteries.

2. Experimental

2.1. Synthesis

The N-CNFs with highly-rough surface were synthesized by an electrospinning process. At first, the precursor solution of PAN (M_w = 52 000) and PVP (M_w = 20 000) was prepared. Secondly, 0.6 g PAN was dissolved in 10 mL dimethylformamide (DMF) to form a faint yellow solution at 60 °C under stirring for 2 h. Lastly, 0.4 g PVP was added to the precursor solution under stirring over 24 h to obtain a mixture solution for electrospinning. The electrospinning process is described below: The precursor solution was loaded into an injector and a voltage of 15 kV was applied by a high-voltage DC power supply unit. A distance of 15 cm between the nozzle tip and the aluminum foil and a flow rate of 0.5 mL/h was applied to electrospinning.

The as-collected nanofibers were stabilized in air at 250 °C with a heating rate of 5 °C/min for 2 h, and then the temperature was further improved to 450 °C with a heating rate of 5 °C/min to remove PVP in nanofibers. Subsequently, the nanofibers were carbonized at 600 °C in an Ar (95 vol%)/H_2 (5 vol%) atmosphere with 2 °C/min for 1 h to obtain N-CNFs with highly-rough surface. For comparison, PAN/PVP nanofibers were synthesized by stabilizing PAN/PVP nanofibers in the air at 250 °C without annealing at 450 °C and then directly carbonized in Ar (95 vol%)/H_2 (5 vol%) atmosphere at 600 °C.

2.2. Characterization

The crystalline structure of the as-prepared N-CNFs were characterized by X-ray diffraction (XRD) (Empyrean, PANanlytical B.V.) equipped with Cu Kα radiation (λ = 0.15406 nm). The morphology and microstructure were observed by scanning electron microscopy (SEM, FEI Quanta-200) and by transmission electron microscopy (TEM, FEI Tecnai G2 F20 S-TWIN) with an accelerating voltage of 200 kV. Brunauer-Emmett-Teller (BET) was used to determine the specific surface area. The surface state and electronic structure were tested by using X-ray photoelectron spectroscopy (XPS) (Kratos AXIS UltraDLD ultrahigh vacuum (UHV) surface analysis system) using Al Ka radiation (1486 eV) as a probe. A thermal gravimetric-differential scanning calorimeter (TG-DSC, Q600, TA Instruments) measurement was used to analyze the thermal decomposition behavior for the N-CNFs in the air atmosphere.

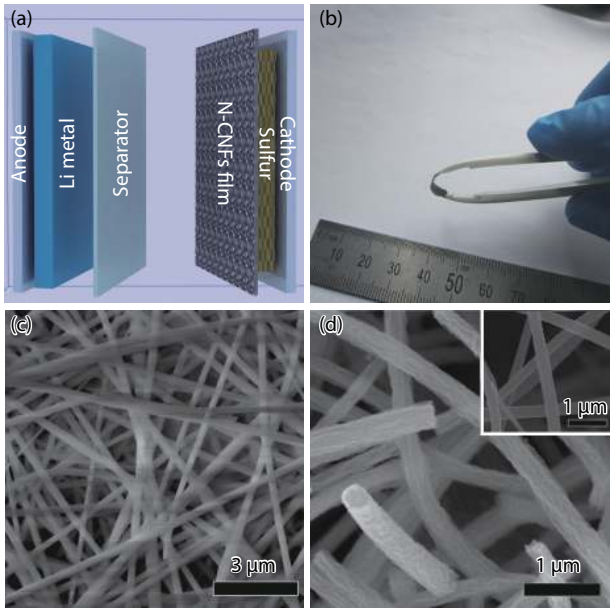

Fig. 1. (Color online) (a) Schematic illustration of a Li–S cell configuration with a N-CNFs interlayer inserting between cathode and separator. (b) Digital image of a N-CNFs interlayer. (c, d) SEM images of the as-spun PAN/PVP nanofibers and the final N-CNFs (inset is the SEM image of the final PAN/PVP nanofibers).

2.3. Electrochemical measurements

The CMK-3/S composite (70% S content) was prepared by grinding CMK-3 and high-purity S powder with a mass ratio of 3 : 7 for 40 min. The active material paste was prepared by mixing CMK-3/S, conductive carbon black and polyvinylidene fluoride (PVDF) with a mass ratio of 7 : 2 : 1 in a N-methyl-2-pyrrolidinone solution. The slurry after grinding was cast onto an Al foil and dried at 60 °C in a vacuum oven for 12 h. The sulfur cathodes and N-CNFs mat were cut into circular disks with a diameter of 12 mm. The mass loading of the sulfur is about 1.4 mg/cm^2 and the weight of a N-CNFs mat is around 0.9 mg. The cathode electrode and the N-CNFs mat were punched into circular discs with the same size. The electrolyte was 1 M lithium bis(trifluoromethanesulfonyl) imde (LiTFSI) in 1,3-dioxolane and 1,2-dimethoxyethane (DME-DOL 1 : 1 v/v). Coin cells of CR2032 were assembled in an argon-filled glove box with Li metal foil, polypropylene separator, N-CNFs interlayer and CMK-3/S cathode electrode in sequence. The galvanostatic charge-discharge tests were conducted on a LAND battery test system (CT2001A). Cyclic voltammetry (CV) measurements were tested by using a CHI 760E electrochemical workstation (ChenHua Instruments Co., China).

3. Results and discussion

Fig. 1(a) illustrates the schematic of a Li–S battery with the functional N-CNFs film as the interlayer, in which the interlayer is sandwiched between the separator and sulfur cathode. The N-CNFs film is utilized to stabilize and trap the polysulfides moving from the cathode to the anode by shuttling effect, aiming to reducing their solubility in organic electrolyte and improving the utilization of the active materials. The

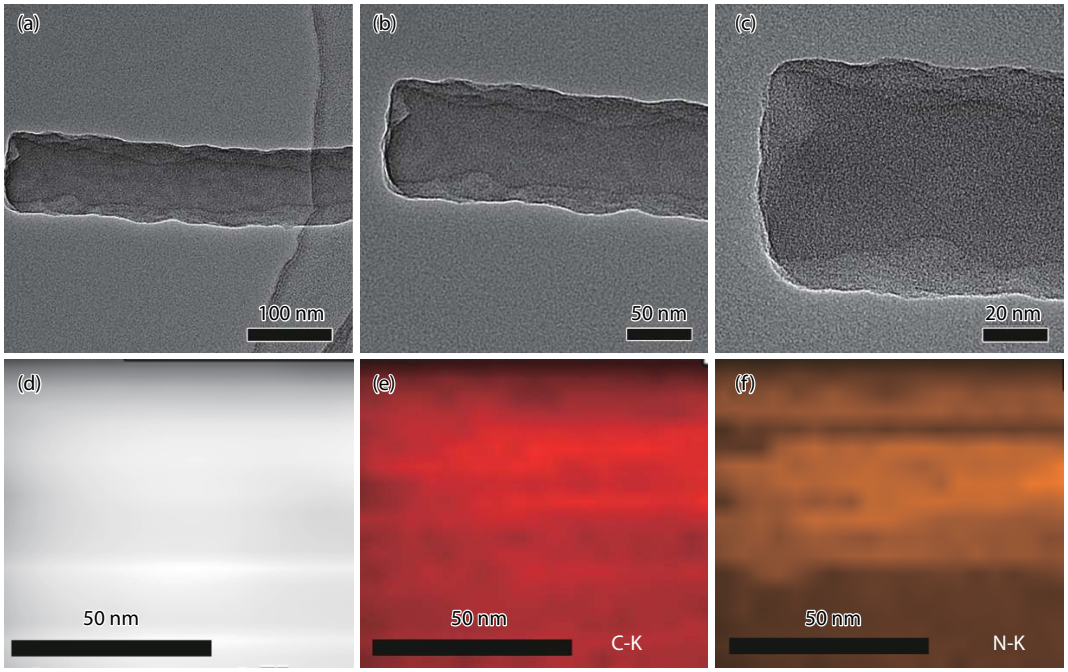

Fig. 2. (Color online) (a–c) TEM images of a single N-CNFs fiber. (d–f) HAADF STEM image and the element mappings for C and N, respectively.

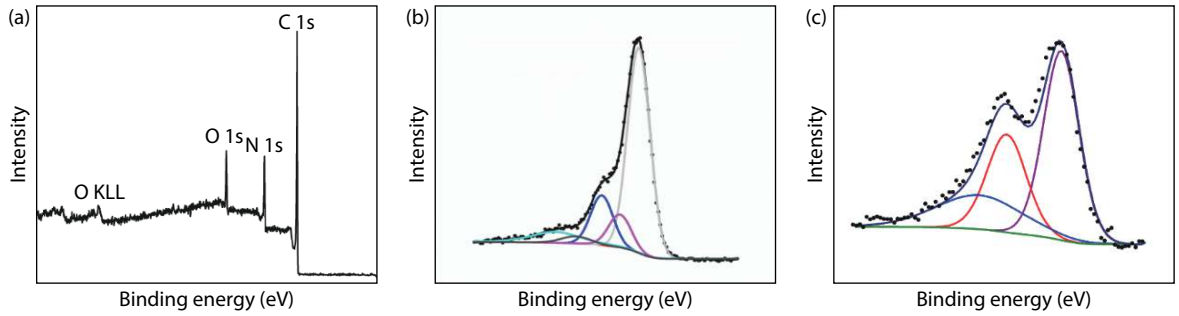

Fig. 3. (Color online) (a) XPS general spectrum of N-CNFs and the corresponding high resolution spectra of (b) C 1s and (c) N 1s.

as-obtained N-CNFs film exhibits excellent flexibility under a bending condition, which ensures the whole structure stability of the interlayer during cycling processes. The N-CNFs mat has the same size as the electrode and its diameter is about 12 mm, as illustrated in Fig. 1(b). Fig. 1(c) is the SEM image of as-spun PVP/PAN nanofibers. The nanofibers are continuous with a uniform diameter around 200 nm and their surface is quite smooth. After stabilization in air and the following carbonization, the as-obtained N-CNFs keeps the fibrous structure with no distinct structural changes compared to the as-spun PVP/PAN nanofibers except for a significantly increased surface roughness as shown in Fig. 1(d). In contrast, the surface of PAN/PVP nanofibers after carbonization is still smooth like the as-spun PVP/PAN nanofibers (inset). The rough surface of N-CNFs would effectively improve the ability of N-CNFs to intercept and adsorb polysulfides.

The detailed microstructures of N-CNFs were further examined by TEM. As shown in Figs. 2(a)–2(c), the diameter of the N-CNFs is 150 nm and the grooves on the nanofiber surface confirm the rough surface. In addition, the high-angle annular-dark-field (HAADF) STEM images of a single nanofiber and element mappings for C and N are illustrated in Figs. 2(d)–2(f). As shown in the element mappings, the nanofibers content C and N elements, confirming the extensive N-doping in the CNFs. The XPS measurement was also performed to further identify the elemental composition of N-CNFs. Fig. 3(a) shows the general XPS spectrum of N-CNFs, which reveals N doping of the N-CNFs film, corresponding to the TEM mapping results. Fig. 3(b) shows the C 1s spectrum and the fitting peaks: C–C in aromatic rings at 284.9 eV, C–N at 285.8 eV, C–O at 286.7 eV, C=O at 288.1 eV, and O=C–O at 289.1 eV. Fig. 3(c) reveals three N 1s peaks at 398.3, 399.9, and 400.8 eV, corresponding to pyridinic, nitrile, and quaternary nitrogen, respectively. N-doping is an effective way to improve the performance for Li–S batteries. From the structure of the N species in the graphene layers, pyridinic N and nitrile could be highly chemically active because these N atoms stay in the edge sites[36]. In addition, these N atoms would immobilize the polysulfides through Li_2S_x–N bonding due to their electronegative character[37]. N-doping of carbon materials can also greatly enhance their electronic conductivity and induce n-type conducting behaviors because N can introduce donor states near the Fermi level[38]. Therefore, N-doping can improve the electronic conductivity of the CNFs interlayer. In addition, the continuous 1D N-CNFs interconnect with each other form a conductive 3D network film, which is beneficial to fast electronic transporting, contributing to improving rate performance for Li–S batteries[39].

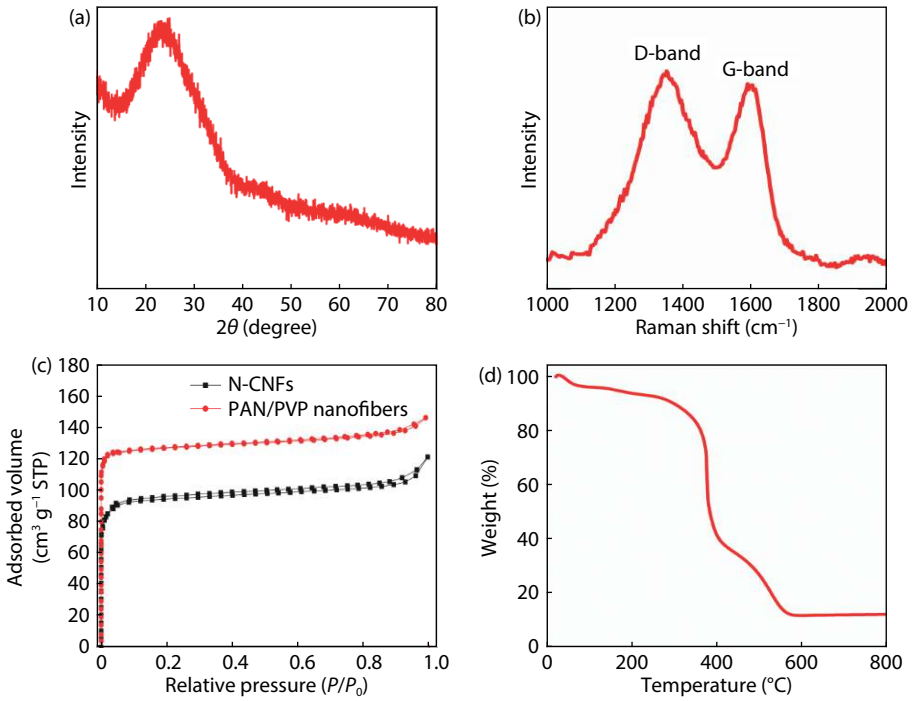

Fig. 4. (Color online) (a) XRD pattern of N-CNFs. (b) Raman spectra of N-CNFs. (c) N_2 adsorption/desorption isotherms of N-CNFs and PAN/PVP nanofibers. (d) Thermogravimetric analysis of N-CNFs in the air.

The structural features of the N-CNFs film were examined by XRD, as shown in Fig. 4(a). There is a broad peak around 24° in the XRD pattern, and it should be corresponding to the typical (002) peak of graphite[40]. This result is also supported by the Raman spectrum of the N-CNFs film (Fig. 4(b)). Two broad peaks at 1346 and 1585 cm^{-1} are related to the structural defects and disorders in the carbon (D band) and E_{2g} vibration mode of the sp^2-bonded carbon atoms (G band), respectively[41]. In addition, the I_D/I_G ratio is about 1.4 indicating its partial graphitization, which is conducive to the transport of electrons between the carbon and the sulfur species. Furthermore, the N_2 adsorption/desorption isotherms (BET) results indicate that the surface area of N-CNFs is larger than that of PAN/PVP nanofibers, which is caused by the roughness surface, as shown in Fig. 4(c). Furthermore, the TGA analysis was used to find a suitable annealing temperature of the PAN/PVP fibers mat though different pyrolysis temperatures of the two kinds of polymers (Fig. 4(d)). From the TGA curve, PVP with a low pyrolysis temperature will be decomposed around 400 °C in contrast to that of 580 °C for PAN. Therefore, heating the PAN/PVP nanofibers film at 450 °C in the air will remove the PVP and get the highly rough surface N-CNFs, after annealing process in Ar/H_2 atmosphere.

The electrochemical performance of Li–S batteries with or without interlayers are compared. Fig. 5(a) shows the charge/discharge voltage profiles of the battery at 0.1 C rate. Two discharge voltage plateaus arise at around 2.25 and 2.1 V, corresponding to two reduction reactions during the discharge process, respectively. In addition, a long voltage plateau appears around 2.3 V is related to a reverse oxidation process. The electrochemical behavior of the Li–S battery with an N-CNFs interlayer is analyzed using CV method. The CV data in the initial four cycles (Fig. 5(b)) are characteristics redox reactions for Li–S batteries. In the cathodic scan, two reduction peaks are appeared at around 2.7 and 2.1 V. The two peaks are representatively associated with an open-ring reduction reaction of S_8 to long-chain Li_2S_n ($4 \leqslant n \leqslant 8$) and a successive decomposition of Li_2S_n into short-chain Li_2S/ Li_2S_2, respectively. During the following anodic scan, a distinct sharp peak, appearing at 2.65 V, corresponds to the oxidation of Li_2S/ Li_2S_2 to Li_2S_8. The redox feature shows no obvious change in the four cycles, indicating highly reactive reversibility and good cyclability of the battery. The cycling performance of the Li–S batteries is plotted in Fig. 5(c). Li–S batteries with interlayers show obvious capacity improvement, comparing to the one without interlayer. In detail, all three batteries can deliver an initial discharge capacity of about 1200 mAh/g, but Li–S batteries with N-CNFs and PAN/PVP interlayers can keep high capacities about 785 and 630 mAh/g, respectively, after 200 cycles. In contrast, Li–S batteries without interlayers show a serious capacity degradation during test, and a very limited capacity of only 20 mAh/g is preserved after 200 cycles. Furthermore, the Li–S battery with N-CNFs exhibits better cycling stability than that of PAN/PVP interlayers. The improved cycling stability is considered to be benefited from the highly-rough surface N-CNFs interlayer which holds a stronger ability to trap sulfur on the cathode side and suppress the polysulfide solubility in the organic electrolyte, comparing to PAN/PVP interlayers. Fig. 5(d) shows rate cycling behaviors of the Li–S battery with an N-CNFs interlayer. The battery displays reversible capacities of 1204, 986, 900, 821, 741 and 573 mAh/g at rates of 0.1, 0.2, 0.5, 1, 2 and 5 C, respectively. Particularly, when the rate turns back to 0.2 C, the capacity recovers to 930 mAh/g, which shows the battery has a strong capacity stability under wide range of rates.

4. Conclusion

We use the highly-rough surface N-CNFs film as flexible in-

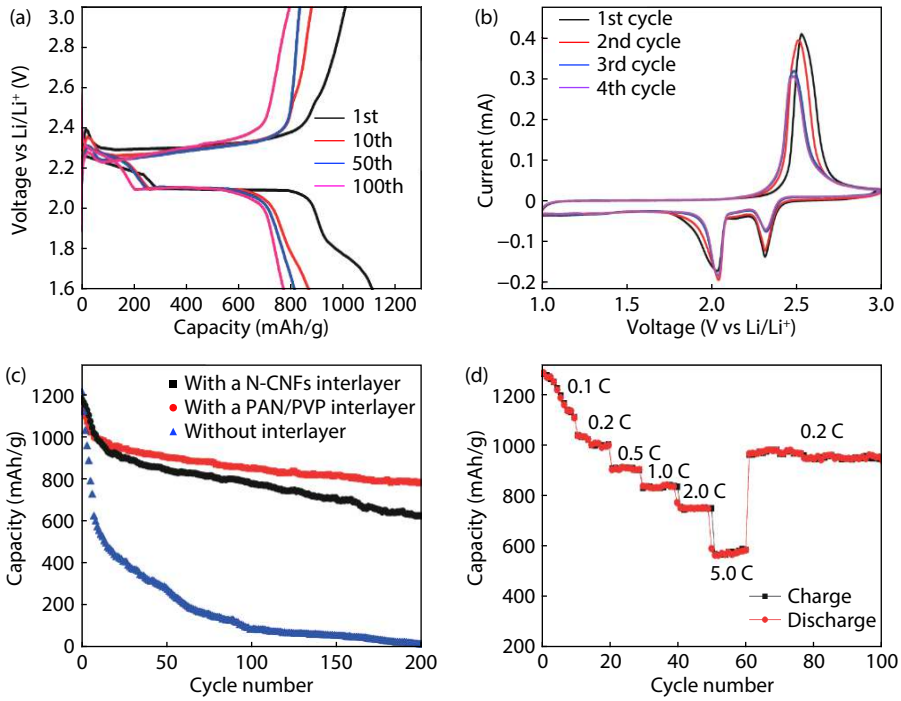

Fig. 5. (Color online) Electrochemical performance of Li–S batteries with N-CNFs an interlayer. (a) Galvanostatic charge/discharge profiles at various cycles of the Li–S cells with a N-CNFs interlayer. (b) CV curves of the initial two cycles from 3.0 V to 1.0 V vs Li^+/Li at a scan rate of 0.05 mV/s. (c) Cycling performance of the Li–S batteries using different interlayers and (d) rate capabilities at various current rates, from 0.1 C to 5 C and back to 0.2 C.

terlayers and apply them in Li–S batteries. The highly-rough surface interlayer provides large surface area to stabilize polysulfides and suppress the solubility in organic electrolyte. Besides, N-doping gives the CNFs film good electrical conductivity, which can improve rate capacity for Li–S batteries. The Li–S battery with an N-CNFs interlayer displays a high discharge capacity 785 mAh/g after 200 cycles and good rate capability of 573 mAh/g at 5 C. The enhanced electrochemical performance demonstrates this highly-rough surface N-CNFs interlayer synthesized by electrospinning is a promising method to fabricate high capability Li–S batteries.

Acknowledgements

The work was supported by the Natural Science Foundation of China (NSFC) (Grant No. U1432249, 21203130) and the Priority Academic Program Development of Jiangsu Higher Education Institutions (PAPD). This work was also supported by the German Research Foundation (DFG: LE2249/5-1).

References

[1] Zhang C, Ma Y, Zhang X, et al. Two-dimensional transition metal carbides and nitrides (MXenes): Synthesis, properties, and electrochemical energy storage applications. Energy Environ Mater, 2020, 3, 29

[2] He Q, Yu B, Li Z, et al. Density functional theory for battery materials. Energy Environ Mater, 2019, 2, 264

[3] Tu W, Wen Y, Ye C, et al. Phase transformation of lithium-rich oxide cathode in full cell and its suppression by solid electrolyte interphase on graphite anode. Energy Environ Mater, 2020, 3, 19

[4] Or T, Gourley S W, Kaliyappan K, et al. Recycling of mixed cathode lithium-ion batteries for electric vehicles: Current status and future outlook. Carbon Energy, 2020, 2, 6

[5] Xu H, Peng C, Yan Y, et al. "All-in-one" integrated ultrathin SnS_2@3D multichannel carbon matrix power high-areal–capacity lithium battery anode. Carbon Energy, 2019, 1, 276

[6] Shin W, Lu J, Ji X. ZnS coating of cathode facilitates lean-electrolyte Li–S batteries. Carbon Energy, 2019, 1, 165

[7] Ding N, Chien S W, Hor T A, et al. Key parameters in design of lithium sulfur batteries. J Power Sources, 2014, 269, 111

[8] Manthiram A, Fu Y, Su Y S. Challenges and prospects of lithium–sulfur batteries. Acc Chem Res, 2013, 46, 1125

[9] Zang Y, Pei F, Huang J, et al. Large-area preparation of crack-free crystalline microporous conductive membrane to upgrade high energy lithium–sulfur batteries. Adv Energy Mater, 2018, 8, 1802052

[10] Zhang S S. Liquid electrolyte lithium/sulfur battery: Fundamental chemistry, problems, and solutions. J Power Sources, 2013, 231, 153

[11] Chung W J, Griebel J J, Kim E T, et al. The use of elemental sulfur as an alternative feedstock for polymeric materials. Nat Chem, 2013, 5, 518

[12] Yin Y X, Xin S, Guo Y G, et al. Lithium–sulfur batteries: electrochemistry, materials, and prospects. Angew Chem Int Ed, 2013, 52, 13186

[13] Chen L, Shaw L L. Recent advances in lithium–sulfur batteries. J Power Sources, 2014, 267, 770

[14] Chen S R, Zhai Y P, Xu G L, et al. Ordered mesoporous carbon/sulfur nanocomposite of high performances as cathode for lithium–sulfur battery. Electrochim Acta, 2011, 56, 9549

[15] Wang G, Lai Y, Zhang Z, et al. Enhanced rate capability and cycle stability of lithium–sulfur batteries with a bifunctional MCNT@PEG-modified separator. J Mater Chem A, 2015, 3, 7139

[16] Park J, Yu B C, Park J S, et al. Tungsten disulfide catalysts supported on a carbon cloth interlayer for high performance Li–S battery. Adv Energy Mater, 2017, 7, 1602567

[17] Li H, Sun L, Zhang Y, et al. Enhanced cycle performance of Li/S battery with the reduced graphene oxide/activated carbon functional interlayer. J Energy Chem, 2017, 26, 1276

[18] Gao T, Le T, Yang Y, et al. Effects of electrospun carbon nano-

fibers' interlayers on high-performance lithium–sulfur batteries. Materials, 2017, 10, 376

[19] Yuan Z, Peng H J, Hou T Z, et al. Powering lithium–sulfur battery performance by propelling polysulfide redox at sulfiphilic hosts. Nano Lett, 2016, 16, 519

[20] Ma G, Wen Z, Wang Q, et al. Enhanced performance of lithium sulfur battery with self-assembly polypyrrole nanotube film as the functional interlayer. J Power Sources, 2015, 273, 511

[21] Jeong T G, Moon Y H, Chun H H, et al. Free standing acetylene black mesh to capture dissolved polysulfide in lithium sulfur batteries. ChemCommun, 2013, 49, 11107

[22] Zhang K, Qin F, Fang J, et al. Nickel foam as interlayer to improve the performance of lithium–sulfur battery. J Solid State Electrochem, 2014, 18, 1025

[23] Ma G, Wen Z, Jin J, et al. Enhanced cycle performance of Li–S battery with a polypyrrole functional interlayer. J Power Sources, 2014, 267, 542

[24] Singhal R, Chung S H, Manthiram A, et al. A free-standing carbon nanofiber interlayer for high-performance lithium–sulfur batteries. J Mater Chem A, 2015, 3, 4530

[25] Zhang Z, Wang G, Lai Y, et al. Nitrogen-doped porous hollow carbon sphere-decorated separators for advanced lithium–sulfur batteries. J Power Sources, 2015, 300, 157

[26] Williams B P, Joo Y L. Tunable large mesopores in carbon nanofiber interlayers for high-rate lithium sulfur batteries. J Electrochem Soc, 2016, 163, A2745

[27] Zeng L, Pan F, Li W, et al. Free-standing porous carbon nanofibers-sulfur composite for flexible Li–S battery cathode. Nanoscale, 2014, 6, 9579

[28] Su Y S, Manthiram A. A new approach to improve cycle performance of rechargeable lithium–sulfur batteries by inserting a free-standing MWCNT interlayer. Chem Commun, 2012, 48, 8817

[29] Kong W, Yan L, Luo Y, et al. Ultrathin MnO_2/graphene oxide/carbon nanotube interlayer as efficient polysulfide-trapping shield for high-performance Li–S batteries. Adv Funct Mater, 2017, 27, 1606663

[30] Wang X, Wang Z, Chen L. Reduced graphene oxide film as a shuttle-inhibiting interlayer in a lithium–sulfur battery. J Power Sources, 2013, 242, 65

[31] Zhou G, Li L, Wang D W, et al. A flexible sulfur-graphene-polypropylene separator integrated electrode for advanced Li–S batteries. Adv Mater, 2015, 27, 641

[32] Liang G, Wu J, Qin X, et al. Ultrafine TiO_2 decorated carbon nanofibers as multifunctional interlayer for high-performance lithium–sulfur battery. ACS Appl Mater Interfaces, 2016, 8, 23105

[33] Sha M, Zhang H, Nie Y, et al. Sn nanoparticles@nitrogen-doped carbon nanofiber composites as high-performance anodes for sodium-ion batteries. J Mater Chem A, 2017, 5, 6277

[34] Demir M M, Yilgor I, Yilgor E, et al. Electrospinning of polyurethane fibers. Polymer, 2002, 43, 3303

[35] Wang L, Yu Y, Chen P, et al. Electrospinning synthesis of C/Fe_3O_4 composite nanofibers and their application for high performance lithium-ion batteries. J Power Sources, 2008, 183, 717

[36] Wang X, Weng Q, Liu X, et al. Atomistic origins of high rate capability and capacity of N-doped graphene for lithium storage. Nano Lett, 2014, 14, 1164

[37] Wang S, Zou K, Qian Y, et al. Insight to the synergistic effect of N-doping level and pore structure on improving the electrochemical performance of sulfur/N-doped porous carbon cathode for Li–S batteries. Carbon, 2019, 144, 745

[38] Hellgren N, Guo J, Såthe C, et al. Nitrogen bonding structure in carbon nitride thin films studied by soft X-ray spectroscopy. Appl Phys Lett, 2001, 79, 4348

[39] Xu J, Wang M, Wickramaratne N P, et al. High-performance sodium ion batteries based on a 3D anode from nitrogen-doped graphene foams. Adv Mater, 2015, 27, 2042

[40] Le T H, Yang Y, Yu L, et al. Polyimide-based porous hollow carbon nanofibers for supercapacitor electrode. J Appl Polym Sci, 2016, 133

[41] Pandey J, Prajapati P, Shimpi M R, et al. Studies of molecular structure, hydrogen bonding and chemical activity of a nitrofurantoin-L-proline cocrystal: a combined spectroscopic and quantum chemical approach. RSC Adv, 2016, 6, 74135